Surface & Coatings Technology 211 (2012) 209–212

Contents lists available at SciVerse ScienceDirect

Surface & Coatings Technology

journal homepage: www.elsevier.com/locate/surfcoat

Roughness studies of NiTi shape memory alloy treated by nitrogen plasma based ion implantation at high temperatures

M.M. Silva [a,b,*], L. Pichon [a], M. Drouet [a], J. Otubo [b]

[a] Institut Pprime, UPR 3346 CNRS-Université de Poitiers-ENSMA, France
[b] Instituto Tecnologico de Aeronautica, ITA, Sao Jose dos Campos-SP, Brazil

ARTICLE INFO

Available online 30 July 2011

Keywords:
NiTi
EBM
Shape memory alloy
Plasma based ion implantation
Roughness

ABSTRACT

The NiTi shape memory alloys (SMA) are employed in various applications, thanks to its specific mechanical properties. However, for many applications, it is interesting to improve its surface mechanical resistance to tribological or chemical attacks. This work aims to analyze the effects of nitrogen plasma based ion implantation (PBII) technique on the surface of NiTi produced by electron beam melting (EBM). The samples were treated for 120 min (550 °C and 770 °C) and 360 min (550 °C), with 16 kV high voltage pulses. The surfaces were analysed by X-ray diffraction (XRD), white light interferometry (WLI) and glow discharge optical emission spectrometry (GDOES). In addition to martensitic and austenitic NiTi, the XRD analysis shows the appearance of titanium nitride TiN and Ni_3Ti phase in the PBII treated samples. Whereas the untreated specimen presents a RMS roughness R_{RMS} around 16 nm, the PBII treatments were shown to increase it, from 44 nm, at 550 °C, to 82 nm at 770 °C. The nitrogen incorporation ranges from 150 nm (at 550 °C, whatever the duration), up to more than 500 nm (770 °C) thanks to temperature activated diffusion. The increase of R_{RMS} may be explained by the sputtering effect but it may be linked to the presence of a buried oxi-nitride phase grown by diffusion at higher temperature.

1. Introduction

The NiTi shape memory alloys (SMA) is a promising material that is widely used in several areas like aerospace, nuclear, automotive, robotics, medical and others areas due to its good mechanical properties, shape memory effect and superelasticity [1,2]. It is highly interesting as a biomedical material, taking into account its properties such as shape recovery when deformed beyond its elastic limit, either by heating (shape memory effect) or by applied load release (pseudoelastic effect) [3,4].

The alloy used in this work (Ti-55.3 wt.% Ni) was produced by ITA group, using the Electron Beam Melting (EBM) process, by which the contamination by carbon is completely eliminated, since melting is done in a water-cooled copper crucible, moreover the contamination by oxygen is minimized thanks to operation in high vacuum with chamber internal pressure less than 10^{-2} Pa [5,6].

Nitrogen Plasma Based Ion Implantation was already shown to be a successful surface modification process to increase the wear resistance of materials [7–9]. PBII is an advanced technique that allows three-dimensional ion implantation in complex shape work-pieces, with no dimensional change of treated components. As no film is deposited, delamination is avoided [10,11].

The roughness is a very important factor for many considered applications, such as dental prosthesis, where it can affects the effectiveness of sliding mechanics and the corrosion behavior of orthodontic components [12,13]. Whereas PBII usually increases the materials roughness, it significantly decreases their friction coefficient [7–9], which is a very important factor of sliding mechanisms too. On the other hand, there are some applications where a higher roughness is required: Wirth C. et al. showed that it helps to stimulate the cell proliferation and it has not any influence on neither the osteoblasts morphology nor their adhesion [14].

2. Experimental Procedures

The NiTi samples disks of 15 mm in diameter and 2 mm thick, produced by EBM process, were polished down to mirror-like quality, down to RMS roughness around 16 nm. The initial ingot production by EBM can be seeing elsewhere [5] and its chemical composition was, 55.3 wt.% Ni, 0.016 wt.% C, 0.070 wt.% O and 0.005 wt.% N. Nitrogen PBII experiments were performed in the home-made TAPIIR set-up (thermally assisted plasma ion implantation reactor), whose scheme was previously described in details [15,16].

The specimens were treated at temperatures of 550 °C or 770 °C, during 120 or 360 min, with the conditions presented in Table 1. The working temperature was reached after 1 h heating under vacuum

* Corresponding author at: Instituto Tecnológico de Aeronáutica, ITA. Divisao de Engenharia Mecanica, Departamento de Materiais e Processos, Praça-Mal. Eduardo Gomes, 50, Vila das Acácias CEP 12228-900, São José dos Campos, SP, Brazil. Tel.: +55 33 05 49 49 67 40, +55 12 3947 5887; fax: +55 12 3947 5887.
E-mail addresses: meg@ita.br, meg.silva@terra.com.br (M.M. Silva).

0257-8972/$ – see front matter © 2011 Elsevier B.V. All rights reserved.
doi:10.1016/j.surfcoat.2011.07.069

Table 1
Conditions of treatment, nitrided thickness and surface RMS roughness of the initial reference sample and the PBII treated samples.

Sample	Pulse high voltage (kV)	Frequency (Hz)	Pulse (μs)	Temperature (°C)	Time (min)	Estimated dose (N /cm²)	Nitrided depth (nm)	RMS Roughness (nm)
#1	Initial NiTi sample							16
#2	16	500 / 200	32–39	550 ± 15	120	1.7E18	150	44
#3	16	500/200	32–39	550 ± 20	360	5.0E18	150	51
#4	16	200	32–39	770 ± 15	120	7.2E17	200 + 300	82

(base pressure below 10^{-4} Pa) with the external furnace surrounding the quartz tube reactor and also helped by additional energy brought by the plasma excitation and, above all, by the ions implantation. It became stable after less than 20 min of operating PBII and was monitored by a thermocouple attached just under the treated samples. The PBII high voltage pulses frequency and length were manually adjusted to maintain a constant operating temperature during the whole treatment. The atomic nitrogen dose implanted in the sample was evaluated from the pulse current, by taking into account only N_2^+ ions in the plasma and a secondary electronic emission coefficient of 4 (previously estimated for the Ti6Al4V material of the sample holder [17]). After the treatment, the samples were allowed to cool down to room temperature under vacuum. The total heat treatment and/or the Ni:Ti ratio modifications due to the nitrided compounds formation may have an important effect on the microstructure, with appearance of various possible phase (Ni_3Ti, $TiNi_3$, Ni_4Ti_3, Ti_4Ni_2O, …) and the possible increase of the martensitic to austenitic phases transitions temperature [18,19]. If the carbon and oxygen content increase the reverse effect could happen once the carbon in excess form TiC and Oxygen may form Ti_4Ni_2O increasing the relation nickel to titanium, that is, the martensitic transformation temperature decreases [20,21].

The samples microstructure was analyzed by X-ray Diffraction (XRD) with $Cu_{K\alpha}$ X-ray wavelength, in Bragg-Brentano geometry. White Light Interferometry (WLI), with a Talysurf CCI 6000 3D optical profiler operating with Mireau interference objectives and white light source, was used to study the surface morphology and roughness. The investigated areas were $900 \times 900\ \mu m^2$ (with X20 objective), with lateral resolution lower than 1 μm and expected vertical resolution of about 0.1 nm. Images were numerically processed using Talymap software V4.1 thus providing 3D profiles of large areas. The nitrogen incorporation and the elemental concentration profiles were measured by Glow Discharge Optical Emission Spectroscopy (GDOES) performed on a Jobin-Yvon-Horiba GD-Profiler.

3. Results

After PBII treatment the surfaces presents dark gold-like color that may be indicative of titanium nitride and/or oxi-nitride formation at the surface. Fig. 1 depicts the XRD diagrams obtained on the different samples. The initial material is not highly homogeneous and presents several peaks, with various intensities depending on the X-ray probed zone. The detected peaks can be attributed to the monoclinic martensitic NiTi phase (JCPDS 35-1281) or to the cubic austenitic NiTi phase which has the more intense peaks [22]. After the PBII treatments, the martensitic proportion has increased as shown by the higher intensity of its relative peaks. Moreover new peaks or shoulders appear at 2θ values of 42.3° (shoulder), 42.65° (shoulder), 43.4° (peak), 44.4° (peak) and 46.5° (peak); most of them are more visible on the XRD diagram of the sample #4, nitrided at 770 °C. The shoulder at 42.3° and the peaks at 43.4° and 46.5° can be attributed to the hexagonal Ni_3Ti (201), (004) and (202) (JCPDS 75-878) respectively; the shoulders at 42.65° may be relative to titanium nitride phases TiN(200). The peak at 44.4° was not identified; it might be relative to an oxide or oxy-nitride phase, or to another kind of Ni_xTi_y phase precipitates (e.g. Ni_4Ti_3 [19], how about Ti_4Ni_2O, complex oxide).

The thickness of nitrided layer, deduced from GDOES profiles (Figs. 2–4), remains very thin, as indicated in Table 1. The PBII treatments at 550 °C (samples #2 and #3) have very similar nitrogen and oxygen chemical profiles (Figs. 2 and 3): nitrogen was incorporated on a depth of about 150 nm; it is detected at deeper depth because of the GDOES sputtering effects. Inside this surface layer, the nitrogen concentration is close to 50 at%. As it was obtained in the untreated sample (profile not shown), the oxygen (resp. carbon) concentration is decreasing from 40 at% (resp.6 at%) to 0 at% within the first 200 nm; oxygen and carbon are likely coming from the native oxide and the surface contamination; they were dragged at so deep depth because of the argon ions irradiation during the GDOES analysis. It has to be noticed that no more nickel is present in this surface layer. Underneath, the nickel content was significantly increased, up to Ni

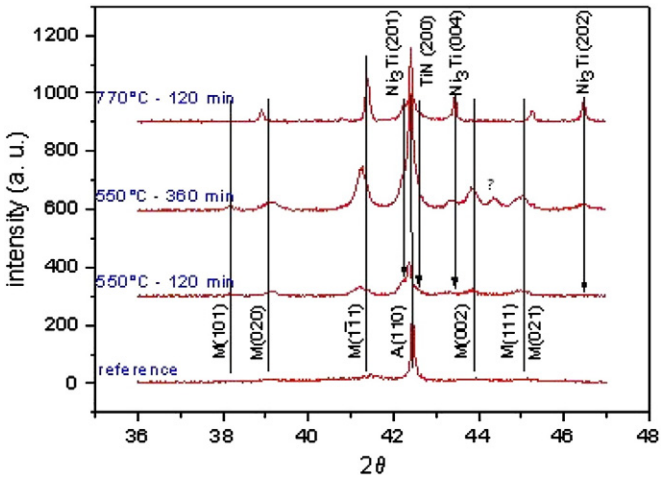

Fig. 1. XRD profiles of untreated and treated samples.

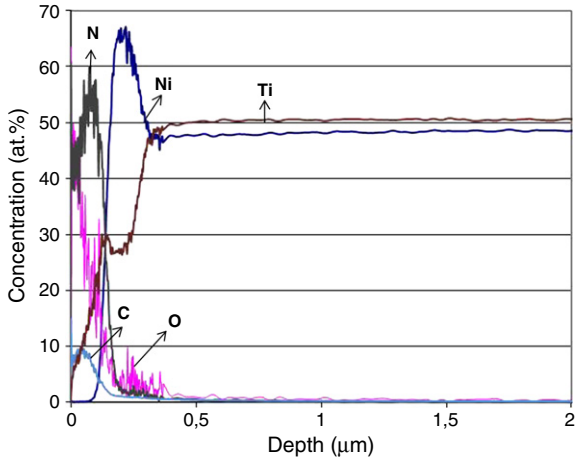

Fig. 2. Elemental concentration profiles obtained by GDOES for sample #2, treated at 550 ± 15 °C, for 120 min.

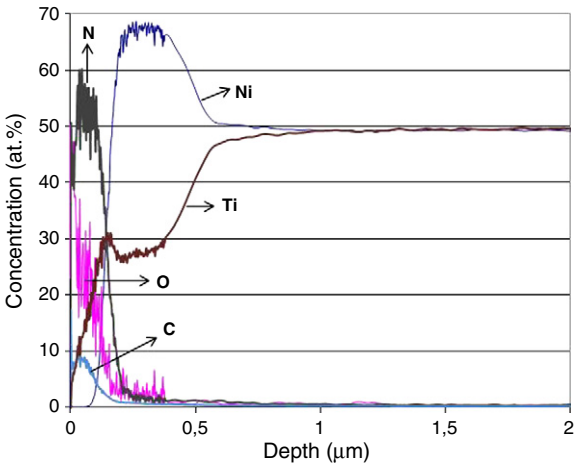

Fig. 3. Elemental concentration profiles obtained by GDOES for sample #3, treated at 550 ± 20 °C, for 360 min.

(70 at%)/Ti (30 at%), instead of Ni (50 at%)/Ti (50 at%) in the bulk. This modification is detected on a thicker thickness with the 6 h treatment (~300 nm) than with the 2 h one (~100 nm). Concerning the sample #4 (770 °C, Fig. 4), a similar nitrogen-rich surface layer is observed on about 200 nm. Below it, there is a titanium oxide layer (~200 nm), with composition $Ti_{0,3}O_{0,55}N_{0,1}C_{0,05}$, without nickel, the oxygen likely originating from the residual pressure. It is followed by an intermediate layer (~400 nm) with high titanium content, increasing nickel content, and decreasing nitrogen and oxygen gradient.

The 3D representations of the samples surface obtained by WLI are shown in Figs. 5–8; the calculated RMS roughness (R_{RMS}) are presented in Table 1. The reference sample shows the smoothest surface (Fig. 5) with R_{RMS} of 16 nm; it increases to 44 nm and 50 nm for the samples nitrided at 550 °C for 2 h and 6 h, and reaches 82 nm for the sample nitrided at 770 °C for 2 h.

4. Discussion

The fact that no nitride phase can easily be evidenced by XRD is consistent with the very thin thickness of the nitrogen-rich layer (≤200 nm). Moreover the relatively high content of oxygen detected by GDOES can let think of the presence of an oxi-nitride phase, instead of pure TiN. It may explain the unaffected XRD peak at 44.4°.

The nickel rich region below the surface layer is consistent with the presence of Ni_3Ti peaks in the XRD diagram of the PBII treated samples [23]. Following the conclusions of Lutz et al. [24], the surface

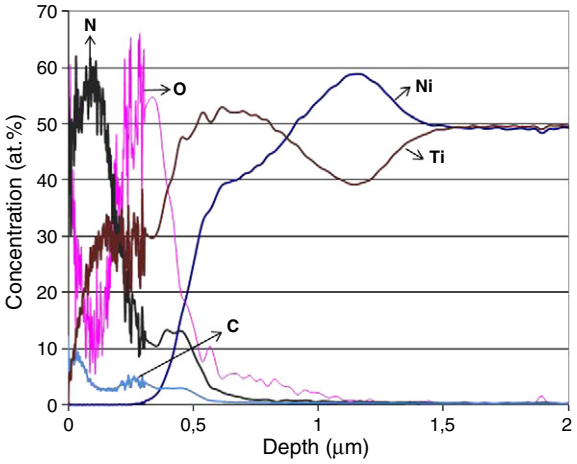

Fig. 4. Elemental concentration profiles obtained by GDOES for sample #4, treated at 770 ± 15 °C, during 120 min.

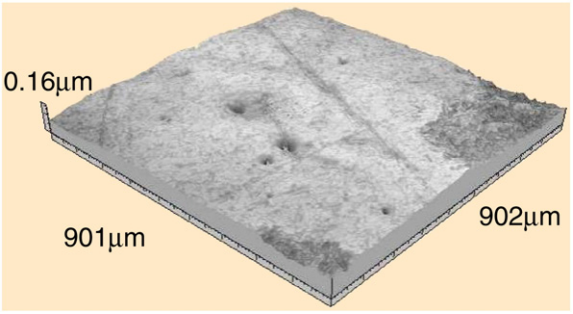

Fig. 5. 3D surface representation of NiTi untreated (#1, reference untreated sample).

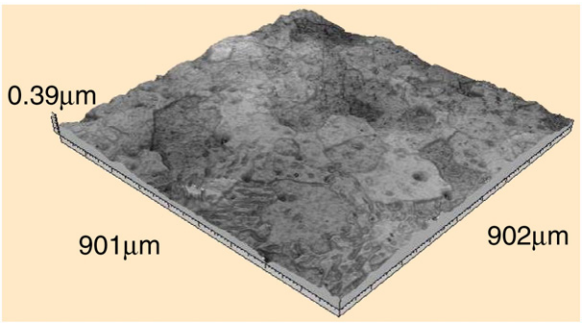

Fig. 6. 3D surface representation of sample #2, treated at 550 ± 15 °C, for 120 min.

nitrided zone, depleted in nickel, is formed by inward diffusion of nitrogen and by the diffusion towards the bulk of the nickel cations. The driving force is brought by the highly favorable nitriding (and oxidizing) reactions of titanium compared to the ones of nickel. The preferential sputtering of nickel due to ions bombardment likely brings a contribution to the depletion in nickel at the surface too. However, if it was the only one reason, the nickel rich zone below the nitrided surface would not exist.

The same nitrided thickness (~150 nm) is obtained with the 2 h and with the 6 h PBII treatments at 550 °C. However, the nickel rich layer below the surface nitride obtained with the 6 h treatment is 3 times thicker than with the 2 h treatment. This is an evidence of the higher amount of nickel which has diffused toward the bulk during this longer time. As the nitrided layer is not thicker, it means that there was a significant sputtering due to the ion bombardment which compensates more or less the diffusion mechanism. The sputtered thickness was naturally thicker with the 6 h treatment than with the 2 h one; it is indeed proportional to the implanted fluence, which is effectively 3 times higher (Table 1). Moreover the roughness is almost the same after 2 and 6 h, which means that it has already reached a steady-state condition after 2 h and does not evolve further because of the sputtering.

Concerning the treatment at 770 °C, similar mechanisms are involved: nitriding of the surface within the implantation range,

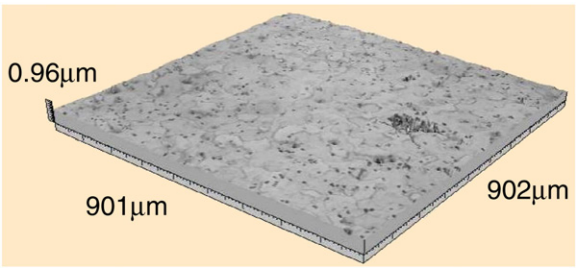

Fig. 7. 3D surface representation of sample #3, treated at 550 ± 15 °C, for 360 min.

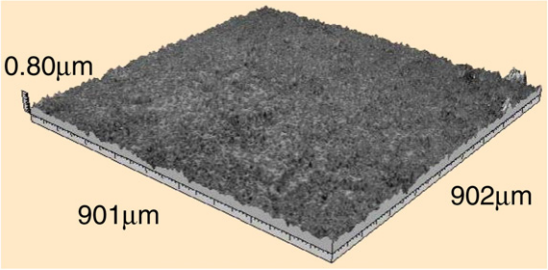

Fig. 8. 3D surface representation of sample #4, treated at 770 ± 15 °C, for 120 min.

surface sputtering (and increase of roughness), nickel diffusion and creation of a buried nickel rich zone. Additionally, because of the higher temperature, diffusion of nitrogen and residual oxygen is enhanced: oxygen and nitrogen are here found in a deeper region, with a decreasing gradient up to about 1 µm. However, it leads preferentially to an oxygen-rich layer likely because of the higher reactivity of titanium with oxygen than with nitrogen.

The growth of this oxi-nitride underlayer is likely responsible of the higher roughness value observed after the 770 °C PBII treatment because of the difference of the atomic volume between the metallic material and the oxinitride. The presence of buried Ni_3Ti precipitates may also involve some elastic or plastic deformation and may participate to the increase of the surface roughness.

5. Conclusions

Surfaces with different values of roughness were obtained with nitrogen PBII treatment of NiTi SMA. Martensitic and austenitic NiTi phases were detected by XRD analysis on the initial NiTi material. The XRD diagrams of the treated samples have indications of TiN and Ni_3Ti phases; a new peak visible at 44.4° might be attributed to oxide or oxi-nitride phases. Concerning the treatments at 550 °C, the roughness (R_{RMS} about 44–51 nm) is relative to the ion sputtering, rapidly reaching a steady-state condition. The nitrided depth remains limited to about 150 nm because of the competition between diffusion and sputtering. With a higher temperature (770 °C) treatment, the roughness is higher: a supplementary contribution is likely brought by the growth of an oxi-nitrided phase, buried underneath the nitrided implanted layer. This new layer is due to the enhanced diffusion at higher temperature and to the higher oxygen reactivity with titanium. Moreover the GDOES chemical profiles have clearly shown a chemical segregation, leading to a nickel-free nitride phase at the surface, and to a nickel enriched layer (likely with Ni_3Ti) before reaching the bulk material. These two aspects should decrease of nickel release from the surface [25] contributing in the sense to use NiTi shape memory alloy as a biomaterial.

Acknowledgements

CAPES: grant 5213096; CNPq: grant 478944/2009-8.

References

[1] K. Otsuka, X. Ren, Intermetallics 7 (1999) 511.
[2] M.F. Chena, X.J. Yanga, R.X. Hua, Z.D. Cui, H.C. Manc, Mater. Sci. Eng. C 24 (2004) 497.
[3] J. Otubo, O.D. Rigo, C. Moura Neto, M.J. Kaufman, P.R. Mei, J. Phys. IV França, 112 (2003), p.873-876.
[4] J. Otubo, O.D. Rigo, C. Moura Neto, P.R. Mei, Mater. Sci. Eng. A 438–440 (2006) 679.
[5] J. Otubo, A.S. Antunes, Mater. Sci. Forum 643 (2010) 55.
[6] O. Winkler, R. Bakish, Vacuum Metallurgy, Elsevier Publishing Company, 1971 (chapter 4).
[7] S. Mändl, A. Fleischer, D. Manova, B. Rauschenbach, Surf. Coat. Technol. 200 (2006) 6225.
[8] X. Liu, S. Wu, Y.L. Chan, P.K. Chu, C.Y. Chung, C.L. Chu, K.W.K. Yeung, W.W. Lu, K.M.C. Cheung, K.D.K. Luk, Mater. Sci. Eng. A 444 (2007) 192.
[9] C.B. Mello, M. Ueda, M.M. Silva, C.M. Lepienski, Wear 267 (2009) 867.
[10] J.R. Conrad, J.L. Radtke, R.A. Dodd, F.J. Worzala, N.C. Tran, J. Appl. Phys. 62 (1987) 4591.
[11] M. Ueda, M.M. Silva, C. Otani, H. Reuther, M. Yatsuzuka, C.M. Lepienski, L.A. Berni, Surf. Coat. Technol. 169–170 (2003) 408.
[12] B. Bourauel, T. Fries, D. Drescher, R. Plietsch, Eur. J. Orthod. 20 (1998) 79.
[13] G.E. Read-Ward, S.P. Jones, E.H. Davies, Br. J. Orthod. 24 (1997) 309.
[14] C. Wirth, B. Grosgogeat, C. Lagneau, N. Jaffrezic-Renault, L. Ponsonnet, Mater. Sci. Eng. C 28 (2008) 990.
[15] L. Marot, M. Drouet, F. Berneau, Straboni, Surf. Coat. Technol. 156 (2002) 155.
[16] L. Pichon, S. Okur, O. Ozturk, J.P. Rivière, M. Drouet, Surf. Coat. Technol. 204 (2010) 2913.
[17] V. Fouquet, L. Pichon, A. Straboni, M., Surf. Coat. Technol. 186 (2004) 34.
[18] H.C. Man, N.Q. Zhao, Surf. Coat. Technol. 200 (2006) 5598.
[19] J. Khalil-Allafi, et al., Acta Mater. 50 (2002) 4255.
[20] J. Otubo, O.D. Rigo, A.A. Coelho, C.M. Neto, P.R. Mei, Mater. Sci. Eng. A 481–482 (2008) 639.
[21] J. Otubo, O.D. Rigo, C.M. Neto, P.R. Mei, Mater. Sci. Eng. A 438–440 (2006) 679.
[22] S. Miyazaki, A. Ishida, Mater. Sci. Eng. A 273–275 (1999) 106.
[23] S. Mändl, J.K.L. Lindner, Nucl. Instrum. Methods B 249 (2006) 355.
[24] J. Lutz, J.K.L. Lindner, S. Mändl, Appl. Surf. Sci. 255 (2008) 1107–1109.
[25] E.N. Camargo, A.O. Lobo, M.M Silva, M. Ueda, E.E. Garcia, L. Pichon, H. Reuther, J. Otubo, J. Mater. Eng. Perform. 20 (2011) 798–801.